Available online at www.sciencedirect.com
ScienceDirect
Geochimica et Cosmochimica Acta 70 (2006) 4921–4932
Geochimica
www.elsevier.com/locate/gca

Quantification of diagenesis in Cenozoic sharks: Elemental and mineralogical changes

Joann Labs-Hochstein [a,b,*], Bruce J. MacFadden [a]

[a] Florida Museum of Natural History, University of Florida, Gainesville, FL 32611, USA
[b] Department of Geological Sciences, University of Florida, Gainesville, FL 32611, USA

Received 24 November 2004; accepted in revised form 13 July 2006

Abstract

Diagenesis of bone during fossilization is pervasive, however, the extent of this process varies with depositional environment. This study quantifies diagenesis of shark vertebral centra through analysis of a suite of physical and chemical characters including crystallinty index (CI), carbonate content, and elemental concentrations. Although shark skeletons are initially cartilaginous, the soft cartilage of the vertebral centra is replaced with carbonate hydroxyapatite during growth. Nine vertebral centra are analyzed from lamnoid (Lamnoidea) sharks ranging in age from the cretaceous to recent using Fourier transform infrared spectroscopy (FT-IR) and inductively coupled plasma mass spectrometry (ICPMS). The variables CI, carbonate content, rare earth element (REE) concentrations, Ca/P, Ba/Ca, Sr/Ba, $(La/Yb)_N$, $(La/Y)_N$, $(La/Yb)_N$ vs. $(La/Sm)_N$, La/Yb, and Ce anomalies elucidate the diagenetic and depositional environments of the seven fossil vertebral centra. The two extant centra demonstrate the initial, unaltered end-member conditions for these variables. Two fossil vertebral centra (*Carcharodon megalodon* and *Isurus hastalis*) demonstrate a strong terrestrial influence during diagenesis (distinctive flattening of shale-normalized REE patterns) that masked the seawater signal. Three centra (*Carcharodon auriculatus*, *Carcharodon angustidens*, and *Creotxyrhina mantelli*) have indications of some terrestrial influx evident by some flattening of the REE patterns relative to seawater. The terrestrial influence in these five shark centra (*C. megalodon*, *I. hastalis*, *C. auriculatus*, *C. angustidens* and *C. mantelli*) are interpreted to represent a primarily nearshore habitat for these species. In contrast, the two *Otodus obliquus* centra have REE patterns that represent the original seawater signal and have no indications of terrigenous input. These results indicate that fossil shark vertebral centra have the potential to understand diagenesis and reconstruct paleooceanographic environments.

1. Introduction

Fossilized vertebrate skeletal tissues, including teeth and bone, have recently received considerable attention as geochemical archives of paleoecological and paleoenvironmental information. In these studies, fossil tooth enamel has been the preferred material for analysis because of the compact, relatively non-porous mineral consisting of >95% hydroxyapatite. In contrast, some interesting studies of broad relevance have been presented using isotopic data from fossil bone (e.g., to reconstruct dinosaur physiology; Barrick and Showers, 1994). However, these studies have come under close scrutiny (Kolodny et al., 1996) because porous bone is more prone to diagenesis than teeth (Wang and Cerling, 1994).

There are certain situations in which fossil bone is either the only skeletal material available for study (e.g., in those vertebrates that lack teeth, such as most birds) or is preferred because certain skeletal elements archive incremental growth. One example of an archive of incremental growth is shark vertebral centra. Although shark skeletons are initially cartilaginous (a soft supporting tissue that does not fossilize), the cartilage is replaced in the vertebral centra with carbonate hydroxyapatite during the growth of the individual. This growth is periodic, and incremental rings are called annuli because of their presumed annular cyclicity, although this is not always the case, (e.g., Branstetter et al., 1987). These growth rings can be easily seen in both

* Corresponding author.
E-mail address: jlabs@ufl.edu (J. Labs-Hochstein).

0016-7037/$ - see front matter © 2006 Elsevier Inc. All rights reserved.
doi:10.1016/j.gca.2006.07.009

modern and fossilized shark centra. During a related research project investigating stable isotopic signatures archived in fossil shark centra (e.g., MacFadden et al., 2004), we became interested in the extent of diagenesis and how it potentially affects the geochemistry of fossil bone.

The purpose of this study is to quantify diagenesis of shark bone through analysis of a suite of physical and chemical characters including crystallinty index (CI), carbonate content, and major, minor, trace elemental concentrations. The sharks are all from the group known as the superfamily Lamnoidea (Cappetta, 1987) which includes the modern great white (*Carcharodon carcharias*) and six closely related extinct species ranging in age from Cretaceous to Pleistocene. The modern shark species are included in this study to provide an unaltered "end-member" in which initial physical parameters and elemental concentrations can be determined. Lamnoid sharks were selected because these sharks are widely distributed in space and time. A broad geographic distribution of fossils should illuminate the effects of different degrees and environments of diagenesis. The vertebral centra were chosen because they are the primary ossified skeletal tissue that fossilizes in sharks (i.e., other than teeth).

1.1. Bone chemistry and diagenesis

Stable isotopes and rare earth elements (REE) of biogenic apatites have been used for paleoclimatic reconstruction, to trace ocean currents and water masses, to quantify redox conditions, for incremental growth studies, and to reconstruct diet (Piper, 1974; Kolodny et al., 1983; Elderfield and Pagett, 1986; Kolodny and Luz, 1991; Lécuyer et al., 1993; Picard et al., 1998, 2002; Shields and Stille, 2001; MacFadden et al., 2004; Pucéat et al., 2004). Partial or complete dissolution, precipitation, recrystallization, and ion uptake by adsorption and diffusion may lead to changes in chemical composition and lattice structure of biogenic apatite (Reiche et al., 2003). As such, the original chemical signatures of biogenic apatites may be modified through diagenesis, resulting in the interpretation of erroneous biological signals (Pucéat et al., 2004).

Modern bone is composed of hydroxyapatite ($Ca_5(PO_4)_6(OH)_2$) that has small crystallites, large surface area (200 m^2/g; Weiner and Price, 1986) and high organic content (~35%, principally collagen and water; Williams, 1989; Carlson, 1990; Koch et al., 1992). The high reactivity of biogenic apatite is due to the small size and high surface area of the bone hydroxyapatite crystallites (Trueman, 1999). Many substitutions are possible for both the anions and cations in biogenic hydroxyapatite (Table 1; Nathan, 1981). In modern biogenic apatites, carbonate (CO_3^{2-}) can substitute for either OH^- (A site) or PO_4^{3-} (B site) but primarily substitutes for the latter (Shemesh, 1990; Lee-Thorp and van der Merwe, 1991; Rink and Schwarcz, 1995). Substitution of carbonate for phosphate can distort the crystal lattice and further decrease the stability of biogenic apatite (Nelson, 1981; Nelson et al., 1983).

Table 1
Some possible substitutions in the apatite crystal structure

Constituent ion	Substituting ion
Ca^{2+}	Na^{2+}, K^{2+}, Sr^{2+}, Mn^{2+}, Mg^{2+}, Zn^{2+},Ba^{2+}, Sc^{3+}, Y^{3+}, REEs, U^{4+}
PO_4^{3-}	CO_3^{2-}, SO_4^{2-}, CrO_4^{2-}, $CO_3{\cdot}F^{3-}$, $CO_3 \cdot OH^{4-}$, SiO_4^{4-}
OH^-	F^-, Cl^-, Br^-, O_2^-

During fossilization the carbonate hydroxyapatite alters to a more stable form of apatite (francolite or carbonate fluorapatite) by losing carbonate and hydroxyl ions and gaining fluoride (Nathan and Sass, 1983; Newsley, 1989; Greene et al., 2004). The loss of carbonate in francolite decreases the defects of the hydroxyapatite lattice, resulting in increased crystal size and stability relative to carbonate hydroxyapatite (Greene et al., 2004).

Through the processes of diagenesis trace element concentrations either increase or decrease relative to those of unaltered bone (Elderfield and Pagett, 1986; Wright et al., 1987; Williams, 1988; Grandjean and Albaréde, 1989; Koeppenkastrop and De Carlo, 1992; Grandjean-Lécuyer et al., 1993; Denys et al., 1996; Hubert et al., 1996; Laenen et al., 1997; Reynard et al., 1999; Trueman, 1999; Starton et al., 2001). Trace elements are most likely incorporated into bone apatite during early diagenesis through substitution. After this initial "recrystallization," trace element signatures appear to be stable and resistant to later diagenesis (Bernat, 1975; Grandjean and Albaréde, 1989; Grandjean-Lécuyer et al., 1993). REE^{3+} ions are similar in size to Ca^{2+}, consequently they readily substitute into the Ca site (Whittacker and Muntus, 1970). Because REE are typically trivalent, introduction of these cations into the Ca site occurs by coupled substitution, for example, $REE^{3+} + Na^+ \leftrightarrow 2Ca^{2+}$.

Adsorption also occurs during diagenesis of biogenic apatite. Binding is usually weak and reversible and therefore ions adsorbed are susceptible to exchange as long as the crystal surface remains exposed. However, if the inter-crystalline porosity is closed during diagenesis, individual crystallite surfaces will be closed to further exchange. Finally, cations (such as Sr^{2+}) may be incorporated into fossil bone via growth of authigenic apatite (Reynard et al., 1999; Trueman and Tuross, 2001). Ultimately, the final trace element composition of the biogenic apatite is controlled by the concentration of trace elements in the system, the apatite–fluid partition coefficient, the chemistry of the burial microenvironment, bone microstructure, and the length of exposure (Trueman, 1999).

1.2. Rare earth elements (REE)

REE research on biogenic apatites is currently focused on the possible uses of the REE signal, determination of the signal source (i.e. environmental, biological, or diagenetic), and the processes of incorporation into the fossil

apatite (Henderson et al., 1983; Fleet, 1984; Grandjean et al., 1987; Wright et al., 1987; Williams, 1988; Trueman, 1996; Trueman and Benton, 1997; Laenen et al., 1997; Reynard et al., 1999; Shields and Stille, 2001; Picard et al., 2002; Trueman and Tuross, 2001). REE in seawater typically exist in the 3^+ oxidation state. One exception is cerium, which can undergo oxidation in seawater from the solvated 3^+ state to the relatively insoluble Ce^{4+} state (deBaar et al., 1985). Under oxic conditions, Ce^{4+} is readily removed from seawater onto particle surface coatings or into authigenic minerals (Sholkovitz et al., 1994; Koeppenkastrop and De Carlo, 1992), resulting in a negative Ce anomaly ($Ce_{anom.}$). In contrast, under reducing conditions Ce^{3+} is typically released back into the water column or pore waters (German and Elderfield, 1990). The oceanic distribution and typical seawater pattern of REE is largely controlled by adsorptive scavenging by settling particles. deBaar et al. (1985) illustrated that in both the Atlantic and Pacific oceans, all REE except Ce increase with water depth.

Bernat (1975) who described icthyolith (fish teeth) in which REE concentrations in from the upper-most 600 cm of ocean-core sediments have a bulk REE pattern similar to overlying waters. These results indicate that biogenic apatites incorporate a REE composition at the sediment/seawater interface during early diagenesis (with little or no fractionation) and are not prone to late diagenetic exchange of REE. Two main theories of REE incorporation into the biogenic apatite at the sediment seawater interface have been proposed. Firstly, some have argued that REE incorporated into biogenic apatite must be transported by and introduced into fossils directly from seawater or porewater (Henderson et al., 1983; Williams, 1988; Trueman, 1996; Trueman and Benton, 1997). However, direct uptake of REE in biogenic apatites from pore waters and/or seawater raises serious problems. Fossil biogenic apatites contain several tens to several hundreds parts per million (ppm) of REE, whereas maximum REE concentrations in pore water and seawater are in the range of parts per billion (ppb) and part per trillion (ppt), respectively (Elderfield and Greaves, 1982; Elderfield and Sholkovitz, 1987). Assuming that the REE are taken up directly through diffusion of pore waters, approximately one ton (10^3 kg) of pore water would be required to give the biogenic apatite enough REE to fit observed concentrations (several tens to several hundreds ppm; Grandjean et al., 1987; Grandjean and Albaréde, 1989; Grandjean-Lécuyer et al., 1993).

Secondly, Grandjean et al. (1987) proposed quantitative uptake of non-detrital REE locally released at the sediment/seawater interface to explain biogenic apatite enrichment. Abundant debris with large surfaces, which easily adsorb large amounts of REE from seawater, are dispersed in the oceans and are known to settle to the ocean floor. Such a rain of REE-rich carriers has been identified in sediment traps (Murphy and Dymond, 1984) and comprises a variety of inorganic (detrital minerals, oxyhydroxides) and organic (pellets, organic debris) phases. The decay of the REE-rich carriers at the sediment/seawater interface associated with biogenic apatites and the resulting reducing conditions eventually cause the dissolution of Fe–Mn oxyhydroxides, which transfer their REE to the recrystallized biogenic apatite. The transfer of REE from oxyhydroxides to biogenic apatites occurs within a rather short period of time (Grandjean and Albaréde, 1989). Upon completion of the early diagenetic processes and once most oxyhydroxides have dissolved, apatite remains the major non-detrital REE repository in sediments (Grandjean and Albaréde, 1989). This extension of Bernat's (1975) model indicates that for biogenic apatites: (1) the primary source of REE is seawater, (2) early diagenetic transfer of REE to biogenic apatites occurs through a short-lived phase consisting of oxyhydroxides and organic detritus, and (3) REE are incorporated within a short period of time and do not undergo late diagenetic exchange.

Variations in host sediments can typically influence the REE compositions of biogenic apatites due to differences in permeability, the REE flux from diagenetic fluids expelled from sediments (diagenetic signal), and organic and oxyhydroxide contents (Grandjean-Lécuyer et al., 1993; Lécuyer et al., 2004). Porewater REE are derived from the surrounding sediments. The higher concentrations of REE in porewaters relative to seawater will allow fluxes of REE from sediments to seawater (i.e., diagenetic fluids that undergo diffusion from sediments into seawater; Elderfield and Sholkovitz, 1987). Terrestrially derived sediments characteristically have shale-normalized REE (REE_N) that are relatively flat and no $Ce_{anom.}$ (particularly from common fine-grained detrital material; Grandjean et al., 1987). Therefore, the REE contents of biogenic apatites deposited in terrestrially derived sediments (clays and sands) typically have flattened REE_N patterns that are intermediate between those of seawater and those of shale (Grandjean et al., 1988; Elderfield et al., 1990). Sediments that precipitate directly from seawater (carbonates and phosphorites) with little or no terrestrial input have diagenetic fluids reflecting the composition of the overlying water column. Biogenic apatite deposited in these types of sediments typically show a seawater REE pattern because the diagenetic signature in the sediments is the same as the overlying water column (Lécuyer et al., 2004). Therefore, the REE signature in fossil biogenic apatites results from a mass balance between the flux of REE from: (1) decaying organic and oxyhydroxides (primary carriers with seawater signature), (2) diagenetic fluids that undergo diffusion from sediments to seawater (diagenetic signature), and (3) rivers (detrital signature; Grandjean and Albaréde, 1989).

There is evidence for REE fractionatation from seawater during incorporation into biogenic apatites. Reynard et al. (1999) generated a model in which partition coefficients of REE between apatites and water for substituted ions were extrapolated from mineral/melt partition data. These were compared with available experimental partition

coefficients for REE adsorption. Reynard et al. (1999) demonstrated that bell-shaped REE patterns (middle REE enrichment) in fossil apatites are due to fractionation with seawater or continental fluids at low temperatures. Therefore, in these cases, the fluid composition can only be determined if the fractionations are known, in which case the fluid composition can be backed out.

Of the numerous geochemical variables that are potentially available to quantify diagenesis, CI, carbonate content, and REE concentrations and ratios seem to be most promising. Crystallinity index, carbonate content, and REE are consistent in modern shark centra and alter during diagenesis; therefore, modern shark centra provide an initial end member. In contrast, as demonstrated below, minor elemental concentrations are highly variable in modern shark centra and are therefore considered less useful in assessing diagenesis.

2. Materials and methods

This study analyzes the geochemistry of nine shark centra (Fig. 1): two modern great whites (*Carcharodon carcharias*) and seven fossil specimens ranging in age from Cretaceous to Pliocene (Table 2). The chemical and mineralogical properties of the nine shark centra were determined by Fourier Transform Infrared Spectroscopy (FT-IR) and Inductively Coupled Plasma Mass Spectrometry (ICPMS). FT-IR is used here to determine crystallinity and estimate carbonate content. FT-IR has advantages over X-ray diffraction (XRD) because only a small amount of sample is required (<1 mg), preparation is easier and produces more accurate results, and carbonate content can be determined. ICPMS allows for the determination of the major, minor, and trace elements in modern and fossil shark centra. ICPMS is a comprehensive technique that is extremely sensitive, with detection limits in the ppb range for many elements in aqueous solution. The high level of accuracy (1–2%) coupled with sensitivity allows analysis at concentrations ranging over more than nine orders of magnitude (Montaser, 1998).

2.1. Fourier transform infrared spectroscopy (FT-IR)

Three ~1 mg samples were drilled with a low-speed Foredom drill from each of the nine centra. Samples were taken along the growth axes, i.e., one from the center, one

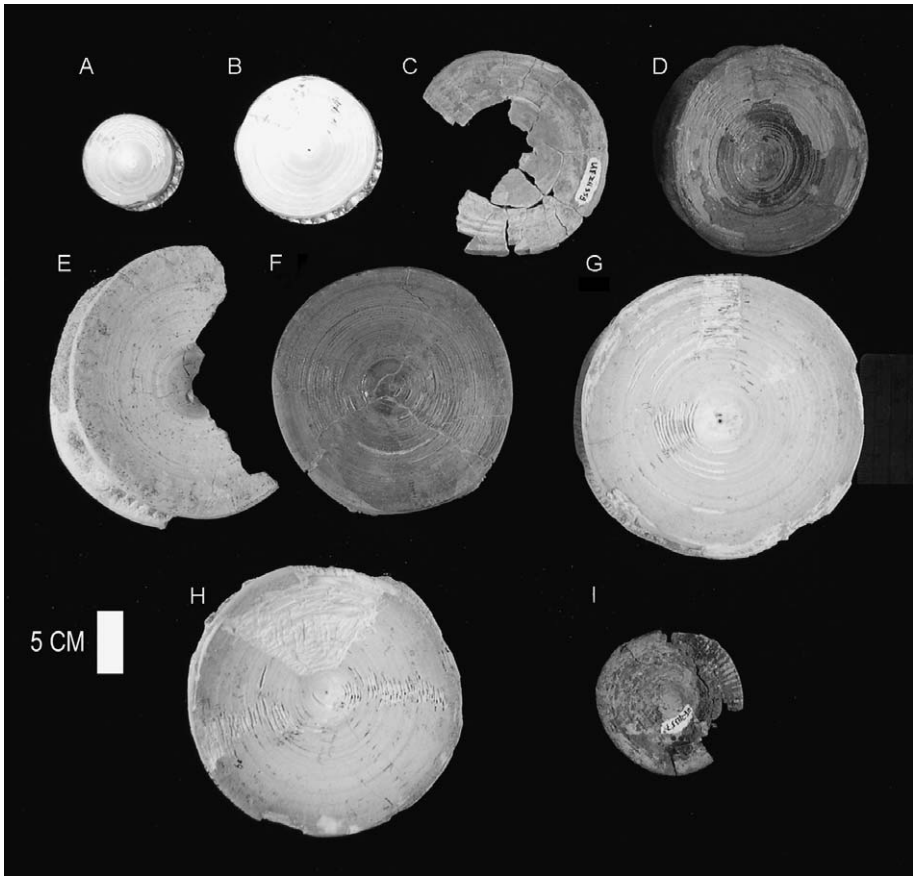

Fig. 1. Nine vertebral centra used in this study. A. *Carcharodon carcharias* (BTO433, Recent, South Africa) B. *Carcharodon carcharias* (UF211351, Recent, USA) C. *Isurus hastalis* (Pliocene, Peru) D. *Carcharodon megalodon* (Miocene, Japan) E. *Carcharodon angustidens* (Oligocene, New Zealand) F. *Carcharodon auriculatus* (Oligocene, Belgium) G. *Otodus obliquus* (Eocene, Morocco) H. *Otodus obliquus* (Eocene, Morocco) I. *Creotxyrhina mantelli* (Cretaceous, USA).

Table 2
Lamnoid (superfamily Lamnoidea, sensu Cappetta, 1987) shark specimens used in this study

Species	Museum ID[a]	Locality	Age	Sediment and depositional environment
Carcharodon carcharias	BTO433	E coast, South Africa	Recent	
Carcharodon carcharias	UF211351	Islamorada, Florida	Recent	
Isurus hastalis	UF211358	Pisco Fm., Peru	Pliocene	Shallow bay sandstone (Brand et al., 2004)
Carcharodon megalodon	SM120A	Saitama Prefecture, Japan	Miocene	Nearshore sandy siltstone (Hayashi et al., 2003)
Carcharodon angustidens	OU22261	Kokoamu Greensand, New Zealand	Oligocene	Shelf glauconitic sand (Ayress, 1993)
Carcharodon auriculatus	EF809A	Brussels Sand, Belgium	Oligocene	Near shore shelf sandstone (Hooyberghs, 1990 and Herman et al., 2000)
Otodus obliquus	UF162732B	Oued Zem, Morocco	Eocene	Shelf phosphorite (Lancelot and Seibold, 1978)
Otodus obliquus	UF162732D	Oued Zem, Morocco	Eocene	Shelf phosphorite (Lancelot and Seibold, 1978)
Creotxyrhina mantelli	UF211357	Niobrara Fm., Kansas	Cretaceous	Shallow epicontinental sea outer shelf chalky shale (Hattin, 1981)

[a] *Abbreviations:* BTO, Natal Sharks Board South Africa; EF, Belgium Museum of Natural History, Belgium; OU, University of Otago Department of Geology New Zealand; UF, Florida Museum of Natural History Florida; SM, Saitama Museum Natural History, Japan.

from the middle, and one from the edge of each centrum. Potassium bromide (KBr) pellets were prepared using the method discussed in MacFadden et al. (2004). Infrared spectra were obtained between 4000 and 400 cm^{-1} on a FT-IR Nicolet 20 SXB Bench housed at the Major Analytical Instrument Center in the UF Material Science and Engineering Department. Interferences from KBr were cancelled by subtracting a standard KBr spectrum from the sample spectra. The crystallite size of biogenic apatite can be determined by calculating the CI from the extent of phosphate peak splitting at 565–605 cm^{-1} in an FT-IR spectrum and is calculated by $CI = (A_{605} + A_{565})/(A_{595})$, where Ax is the absorbance at wave number x (Shemesh, 1990), assuming a straight baseline between 700 and 500 cm^{-1}. Apatites with larger, more ordered crystals show greater separation of these peaks and a higher CI (Shemesh, 1990; Wright and Schwarcz, 1996). An estimate of the carbonate content is given by the absorption ratio of the height of the carbonate peak at 1428 cm^{-1} to the height of the phosphate peak at 1042 cm^{-1} of the FT-IR spectrum (Featherstone et al., 1984; Lee-Thorp and van der Merwe, 1991; Stuart-Williams et al., 1996; Wright and Schwarcz, 1996).

2.2. Elemental analysis (ICPMS)

Approximately 6 mg of bulk sample was drilled with a slow-speed Foredom drill from each of the nine centra. Exactly 5 mg of each sample were weighed out and placed into 3 mL Savillex vials, dissolved in 1 mL of 3 M HNO_3, and heated overnight. Samples were allowed to cool and then were dried on a hot plate. Next, 2 mL of 1% HNO_3 were added, heated overnight, and allowed to cool. Samples were analyzed on an element 2 high resolution inductively coupled plasma mass spectrometer (HR-ICP-MS) at the Center for Trace Element Analysis at the University of Southern Mississippi. Only seven of the 14 REE (La, Ce, Nd, Sm, Gd, Dy, and Yb) were analyzed because these seven are used most often when analyzing diagenetic signals in biogenic apatites. All samples were corrected for: (1) for instrumental drift based on internal machine standards that were analyzed during the run [initial quantification based on comparing the corrected ion counts of the samples with ion count for the standards], (2) ion counts to a constant response to the known amount, and (3) a blank. Rare earth elemental concentrations are shale-normalized to PAAS (Post-Archean Australian Shale Standard) in order to illuminate enrichment-depletion trends relative to average crust (e.g., Grandjean et al., 1988; Elderfield et al., 1990; Grandjean-Lécuyer et al., 1993; Reynard et al., 1999; Trueman and Tuross, 2001). The $Ce_{anom.}$ was calculated from $Ce_{anom} = Log[3Ce_N/(2La_N + Nd_N)]$ (Elderfield and Greaves, 1982).

3. Results

3.1. Mineralogical changes

FT-IR spectra of the modern and fossil shark centra are shown in Fig. 2. Both the modern and fossil samples have the same characteristic absorption bands as the FT-IR spectra of synthetic apatites containing CO_3^{2-} at both A- and B-sites (Bonel, 1972). The FT-IR spectra for modern specimens are characterized by large H_2O bands (which usually mask the OH^- band at 3567 cm^{-1}) and the presence of organics represented by the three amide group bands (amide I 1660 cm^{-1}, amide II 1550 cm^{-1}, and amide III 1236 cm^{-1}). The FT-IR spectra for the fossil specimens are characterized by reduced H_2O bands and absence of one or more of the amide group bands (Fig. 2). There are three prominent phosphate (PO_4^{3-}) absorption bands (with the main absorbance band at 1041 cm^{-1} and a doublet at 605 and 568 cm^{-1}) (Shemesh, 1990). In the modern specimens, the 605 cm^{-1} absorption band has a smaller intensity than the 568 cm^{-1} band, whereas in fossil specimens the 605 cm^{-1} band has a greater intensity than the 568 cm^{-1} band (Fig. 3). The modern specimens have a mean CI of 2.83. In contrast, the CIs of fossil specimens are higher, with a range from 3.19 to 5.39 (Table 3; Fig. 4). B-type carbonate substitution (replacement of $PO4^{3-}$ by CO_3^{2-}; Shemesh, 1990; Dahm and Risnes,

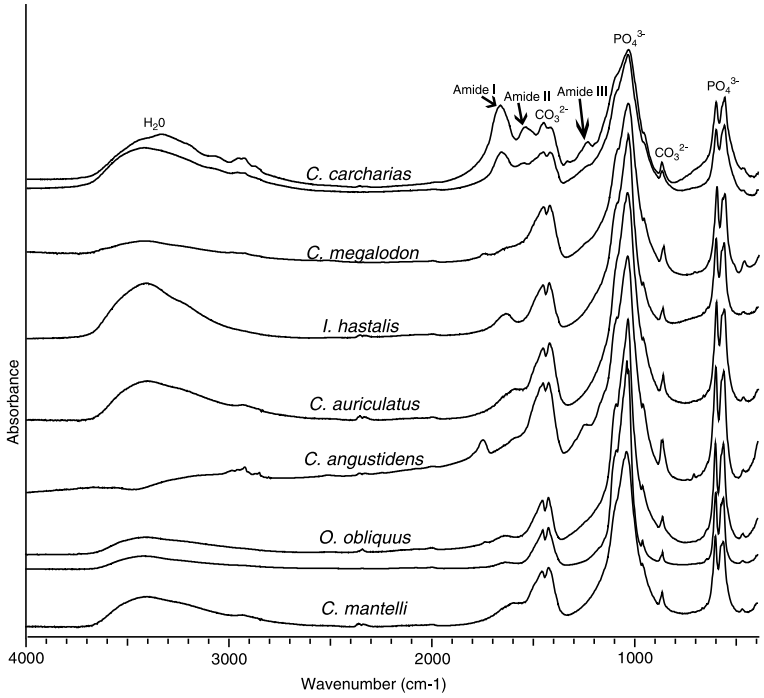

Fig. 2. FT-IR spectra of all nine shark vertebral centra illustrating the differences from modern (top two) to fossil biogenic apatites.

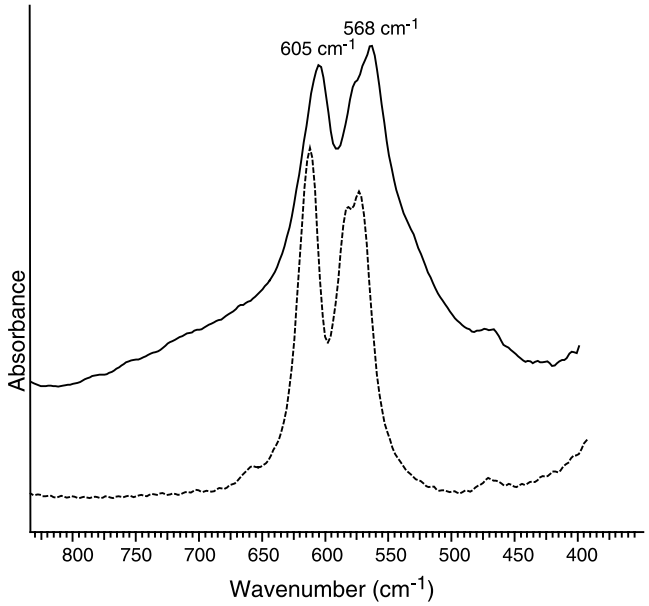

Fig. 3. FT-IR spectra from 400 to 850 cm^{-1}, illustrating the $\gamma 4$ PO_4^{3-} band differences between modern (solid line) to fossil (dashed line) shark centra.

1999) is represented by a set of absorption bands at 1460, 1428, and 870 cm^{-1}. Carbonate content is much greater in modern specimens (0.35 and 0.43) than fossil specimens (range from 0.10 to 0.29) (Table 3; Fig. 4). The lack of the 713 cm^{-1} absorbance band in all samples indicates that there is no authigenic calcite present, and the 1092 cm^{-1} band, which is found only in the fossil specimens, demonstrates the presence of fluorine (Fig. 2).

3.2. Elemental concentration

The effects of diagenesis on elemental concentrations can be assessed by comparing the modern unaltered centra with the altered fossil centra. This is illustrated by the isocon plots (Grant, 1982) in Fig. 5. The linear trends (labeled isocon in Fig. 5) are the mean of the two modern shark centra elemental compositions and represent no elemental loss or gain during diagenesis. The modern major and minor elements vary significantly (Table 3), therefore the gray shaded area in Fig. 5 (Top) represents the range for the isocon. Most of the fossil sharks have Ca, P, Zn, Si, Pb, and B concentrations comparable to the modern sharks (Fig. 5, Top). Three fossils have minor element concentrations of Mg, Sr, and Pb within the modern range (Fig. 5, Top). No fossil specimens have Na, Fe, Al, and Ba concentrations within the modern range (Fig. 5, Top). As seen in Fig. 5 (Middle), diagenesis results in enrichment of Y, U, and REE of the fossil specimens relative to the modern specimens. Fig. 5 (Bottom) shows that the Ba/Ca ratios for the fossils are higher than those of modern sharks because diagenesis has significantly enriched Ba (one to two orders of magnitude greater in fossils than modern shark centra). The fossil Ca/P ratios are slightly higher (0.2–0.5) than modern sharks (Fig. 5, Bottom), which suggest that little or no authigenic apatite has been added during diagenesis.

The REE_N of the shark centra are enriched relative to seawater by about 10^6 to 10^7 (Fig. 6), but the overall patterns for the modern shark centra, and fossil *Otodus obliquus*, *Carcharodon angustidens*, and *Creotxyrhina mantelli* are similar. The REE_N patterns of *Carcharodon megalodon* and *Isurus hastalis* do not resemble seawater but are shale-like.

Table 3
Geochemical and mineralogical data of the nine shark vertebral centra

Specimen	Ca	P	Mg	Na	Zn	Fe	K	Sr	Al	Si	Mn	Ba	Pb	B	Y
C. carcharias (BTO433)	73202.72	59982.29	1752.92	4053.43	904.81	177.22	1133.63	352.49	266.01	28.79	4.80	1.47	9.11	9.10	0.56
C. carcharias (UF211351)	131144.18	115697.43	4239.83	3446.91	2318.75	523.90	314.31	644.75	189.56	1663.73	12.40	1.98	47.03	23.67	0.62
I. hastials	179681.8	132370.77	5234.07	18385.18	449.63	3408.42	2242.55	1031.19	2999.15	118.19	494.58	30.58	13.65	46.98	9.94
C. megalodon	129279.7	78068.01	1521.44	1540.86	575.48	2790.39	239.2	1716.62	2592.67	543.98	667.91	444.4	9.85	49.75	16.14
C. auriculatus	88019.48	61402.78	2027.38	1879.76	1417.02	957.9	183.95	519.99	373.34	953.66	31.74	26.17	29.7	24.52	75.95
C. angustidens	101257.9	61242.34	489.84	1600.81	18.78	883.87	588.53	512.99	568.73	117.64	11.03	24.58	2.58	17.91	21.11
O. obliquus (UF162732B)	159115.68	116988.64	1029.25	3260.41	942.44	133.00	98.96	653.50	149.48	0.00	3.78	62.89	8.11	17.46	31.64
O. obliquus (UF162732D)	186700.89	130473.94	1149.30	37458.43	853.61	113.13	86.01	791.96	106.35	0.00	3.21	76.95	7.96	21.55	32.89
C. mantelli	89909.63	58346.77	648.59	1151.19	516.81	1109.51	145.94	1326.46	553.60	0.00	10.19	283.71	4.72	19.97	98.90

Specimen	La	Ce	Nd	Sm	Gd	Dy	Yb	REE Total	U	Ca/P	$Ce_{anom.}$	CI	Carbonate content
C. carcharias (BTO433)	0.23	0.09	0.14	0.02	0.04	0.04	0.03	1.15	0.28	1.20	−0.70	2.82	0.43
C. carcharias (UF211351)	0.30	0.57	0.34	0.07	0.07	0.09	0.04	2.11	0.27	1.10	−0.10	2.83	0.34
I. hastials	15.04	22.65	9.93	1.85	1.55	1.31	0.97	63.23	6.66	1.40	−0.1	4.3	0.14
C. megalodon	23.78	41.26	16.22	3.37	3.29	2.59	1.03	107.68	1.59	1.70	−0.1	5.39	0.1
C. auriculatus	104.39	128.85	75.73	13.37	14.71	10.25	3.8	427.05	24.84	1.40	−0.2	3.41	0.24
C. angustidens	12.46	13.29	10.85	2.16	2.36	2.19	1.01	65.43	32.9	1.70	−0.2	3.6	0.3
O. obliquus (UF162732B)	14.19	3.79	6.57	1.26	1.92	2.07	1.86	63.30	48.05	1.40	−0.90	4.55	0.17
O. obliquus (UF162732D)	15.48	3.76	6.88	1.29	1.98	2.19	2.00	66.47	57.92	1.40	−0.90	4.55	0.17
C. mantelli	66.39	91.75	39.43	7.40	8.63	9.99	6.34	328.83	27.26	1.50	−0.10	4.02	0.21

Elemental concentrations in ppm. Crystallinity index (CI) and carbonate content were calculated from FT-IR spectra.

Fig. 4. Carbonate content (C/P) vs. Crystallinity index (CI) of the nine shark vertebral centra.

All samples have a negative $Ce_{anom.}$ (Table 3), with samples *C. carcharias* (BTO433) and *O. obliquus* being most negative (−0.73 and −0.85, respectively). The modern specimen UF211351, which was caught off the east coast of Florida, has depleted heavy REE (HREE), higher Ce concentration, a small negative $Ce_{anom.}$, and a lower $(La/Sm)_N$ ratio than BTO433 (Figs. 6 and 7). The fossil specimen *O. obliquus* is slightly enriched in HREE and has a similar REE_N pattern to *C. carcharias* (BTO433) and seawater but with enriched concentrations (Fig. 6A). *O. obliquus* is the only sample that has a $(La/Sm)_N$ ratio greater than *C. carcharias* (BTO433), while all other fossil samples have $(La/Sm)_N$ ratios lying between those of the modern specimens (*C. carcharias*; Fig. 7). The fossil specimens *Carcharodon auriculatus*, *C. angustidens*, and *C. mantelli* have similar REE_N patterns to *C. carcharias* (UF211351) and seawater but show some flattening of the REE_N patterns relative to seawater (Fig. 6B and C). *C. auriculatus* and *C. megalodon* are slightly depleted in HREE, whereas *I. hastalis* has a flat pattern (Fig. 6C and D).

The expected fractionation effects from adsorption and substitution can be depicted in a plot of $(La/Yb)_N$ against $(La/Sm)_N$ (Fig. 7). The La/Sm ratio is little affected by adsorption but will increase through substitution. Conversely, the La/Yb ratio is little affected by substitution but will increase if the adsorption dominates (Reynard et al., 1999). The modern specimen *C. carcharias* (BTO433) has $(La/Sm)_N$ and $(La/Yb)_N$ ratios of 1.5 and 0.5, respectively, which overlap with oceanic water ratios. The other modern specimen, *C. carcharias* (UF211351) and fossil specimen *C. angustidens* have $(La/Sm)_N$ and $(La/Yb)_N$ ratios of 0.6 and 0.6, 0.8, and 0.8, respectively, which overlap with coastal water ratios. The fossil specimens *C. auriculatus*, *I. hastalis*, and *C. megalodon* all have higher $(La/Yb)_N$ ratios (1.3, 1.9, and 1.5) than all other specimens and seawater. Another fossil specimen, *O. obliquus*, has a higher $(La/Sm)_N$ ratio (2.0) than seawater and has a $(La/Yb)_N$ ratio (0.6) that overlaps with coastal

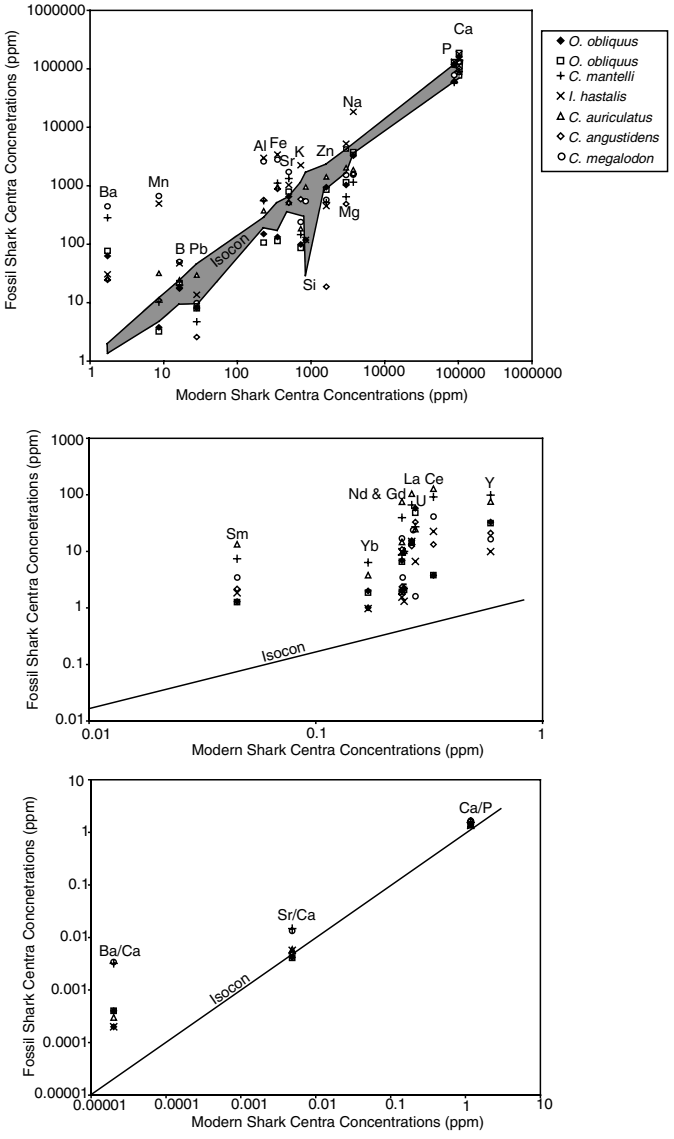

Fig. 5. Isocon plots (Grant, 1982) depicting variations in fossil elemental concentrations and ratios due to diagenesis. In the top plot the shaded area (isocon) represents the variation between the elemental concentrations in the two modern shark centra. The isocon lines in the middle and bottom plots are the mean of the elemental concentrations in the two modern shark centra.

waters. Finally, the fossil specimen, *C. mantelli* has a $(La/Yb)_N$ ratio (0.7) that is higher than oceanic water and a $(La/Sm)_N$ ratio (1.3) that is higher than coastal waters. The differences in the REE_N patterns and ratios have significance for interpretations of both diagenesis and paleoceanography as will be described below.

4. Discussion

4.1. Mineralogical characterization of centra

In contrast to the modern specimens, the fossils have lost most, if not all, of their organic content through diagenesis and therefore contain less absorbed (3430 cm^{-1} band) and structural H_2O (3330 cm^{-1} band; Holcomb and Younf, 1980; Michel et al., 1995). The weak intensity of the absorption band near 1660 cm^{-1}, corresponding to *v*CONH of the amide group (amide I), and the absence of the two other amide bands (amide II and III) signify a significant loss of organics in the fossils (Reiche et al., 2003). The FT-IR spectra of the modern specimens show prominent amide I, II, and III bands and thus indicate the presence of organic matter (Reiche et al., 2003).

When comparing the two modern specimens, the CIs are similar, but the carbonate content differs, with the South African *C. carcharias* (BTO433) having a higher carbonate content than the one from Florida. This may be due to: (1) natural variability within a shark species, or (2) overlapping absorption peaks that have both carbonate substitution in the A-site for OH^- and B-site for PO_4^{3-} (i.e., peaks 1460 and 870 cm^{-1}) that are not included in the estimation of carbonate content. Because the carbonate content is only normalized by a phosphate peak, the use of A-site substituted carbonate would not be an accurate representation of carbonate content. Typically in modern specimens the OH^- band at 3567 cm^{-1} is masked by the water bands and is completely absent in fossil specimens (Fig. 2), making it difficult to use as a normalizer. Lower C/P and higher CI in fossil specimens (Fig. 4) indicate diagenetic loss of carbonate during recrystallization and possibly dissolution of the mineral phase.

4.2. Implications for diagenetic and biological signal reconstruction

The two modern shark specimens (Fig. 6) have similar REE_N patterns to seawater; however, *C. carcharias* (BTO433) from South Africa has a more negative $Ce_{anom.}$ and greater HREE enrichment than UF211351 from Florida. The larger negative $Ce_{anom.}$ in *C. carcharias* (BTO433) may indicate that sharks from the coast of Africa live and/or spent most of their time at greater depths than sharks from the east coast of North America.

The REE_N patterns for the fossil specimens (Fig. 6) may be divided into four groups. The first group, which includes the two *O. obliquus* specimens, has seawater-like REE_N patterns similar to the modern shark pattern of BTO433 (Fig. 6A) and shows a minimum at Sm (disregarding Ce) and a large $Ce_{anom.}$ (greater than −0.3). The seawater-like pattern indicates that REE enrichment during diagenesis involved quantitative uptake of REE without fractionation. Reynard et al. (1999) demonstrated that MREE enrichment (bell-shaped pattern) is related to recrystallization of biogenic apatite and, therefore, is controlled by the fractionation of REEs between apatite and seawater or porewaters. Thus, there was no absorption taking place and no indication of a diagenetic signature (flattening of the REE_N patterns; Grandjean et al., 1987), and the REE did not undergo fractionation with seawater (i.e., there is no MREE enrichment or bell shaped pattern; Reynard et al., 1999). The La/Yb ratio of ~7 and a larger negative

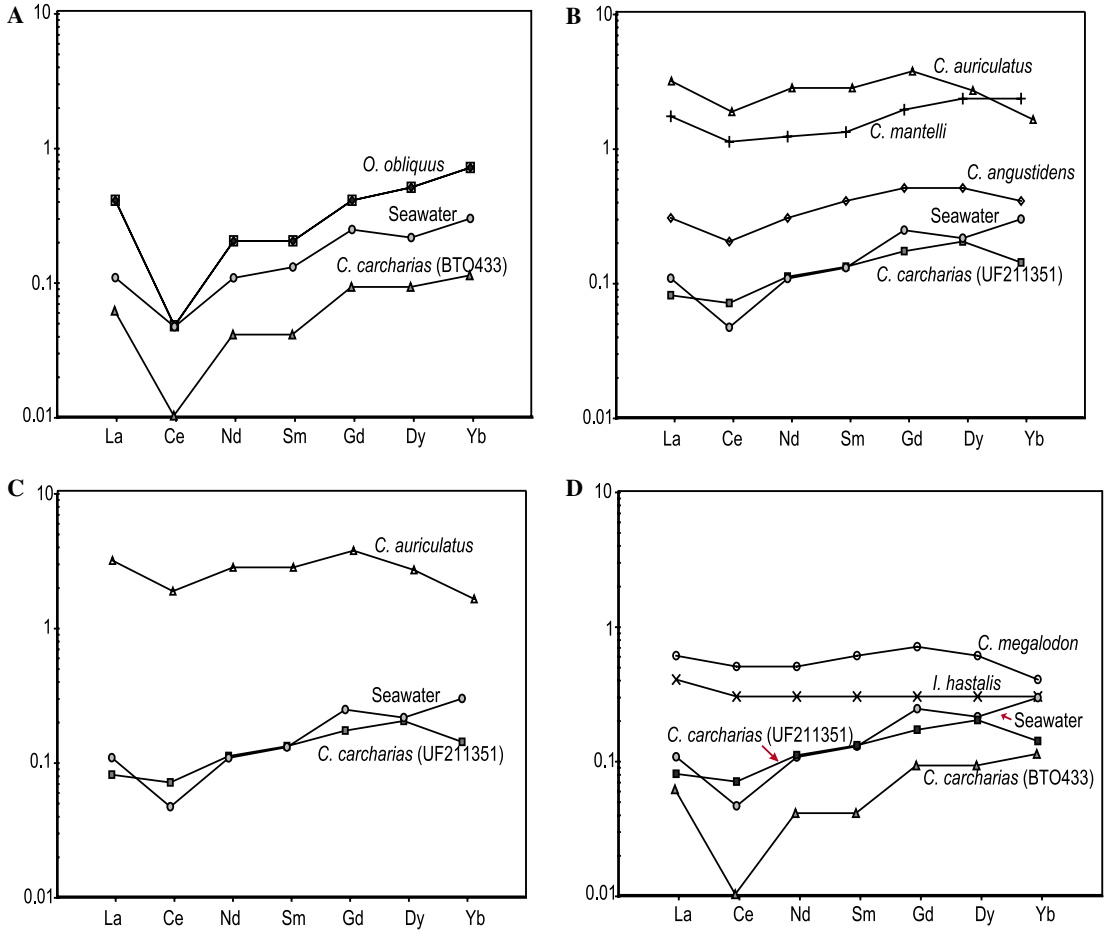

Fig. 6. REE_N (normalized to PAAS) of the nine vertebral centra divided into four diagenetic groups. Seawater is mean seawater (Elderfield and Greaves, 1982) and multiplied by 10^6 and modern specimens UF211351 and BTO433 are multiplied by 10^1.

$Ce_{anom.}$ indicates deposition in an environment with a deepwater influence (Grandjean et al., 1987; Grandjean et al., 1988; German and Elderfield, 1990; Piepgrass and Jacobsen, 1992). Cappetta (1981) showed that early Eocene (Ypresian) fish associations from Oued Zem in the Ouled Abdoun basin (i.e., the location of *O. obliquus*) indicate greater depth than previous geologic periods. This is consistent with results from DSDP Leg 41 off the Moroccan coast that have identified the onset of abundant chert deposition during the early Tertiary reflecting input of cold bottom water (Lancelot and Seibold, 1978). All this evidence supports an influence of deepwater during the diagenesis of *O. obliquus*. The original REE signal of the two *O. obliquus* centra have been replaced during diagenesis at/or near the sediment/seawater interface with the deeper seawater signal present at time of deposition of the centra.

The second group (Fig. 6B), which includes *C. angustidens* and *C. mantelli*, have REE_N patterns similar to that of the modern shark UF211351 and close to seawater but with some flattening. Both *C. angustidens* and *C. mantelli* have a minimum at Nd (disregarding Ce), no MREE enrichment (which indicate fractionation), $(La/Yb)_N$ and $(La/Sm)_N$ ratios that fall within or just outside of coastal waters (Fig. 7), and small negative $Ce_{anom.}$ (less than −0.3). *C. angustidens* from New Zealand was deposited in glauconitic shelf sand (Kokoamu Greensand) at a shallow-water depth estimated to be 50–100 m. The presence of glauconite indicates slow sedimentation and low inputs of detritus from land. During the Oligocene, New Zealand was generally of low elevation and almost fully submerged (Ayress, 1993); therefore, the diagenetic signature was only slightly influenced by terrestrial sediments. This interpretation is supported by minor flattening of the *C. angustidens* REE_N pattern relative to seawater. *C. mantelli* was deposited in the Smoky Hill Chalk Member of the Niobrara Formation at a water depth estimated between 30 and 180 m (Hattin, 1981). The sediments of the Smoky Hill Chalk Member are from the mid to outer shelf of the Cretaceous epicontinental seaway. Only a small amount of terrestrial input has influenced the diagenetic signature, which accounts for the slight flattening of *C. mantelli* REE_N pattern. Neither *C. angustidens* nor *C. mantelli* show any indication of REE fractionation ("bell-shaped" REE_N pattern). The third group, which consists of *C. auriculatus*, shows a minimum in HREE, a REE_N pattern similar in some characters to both seawater and the modern shark pattern of UF211351 (Fig. 6C), and no MREE enrichment. The third group is also characterized by a $(La/Yb)_N$ ratio

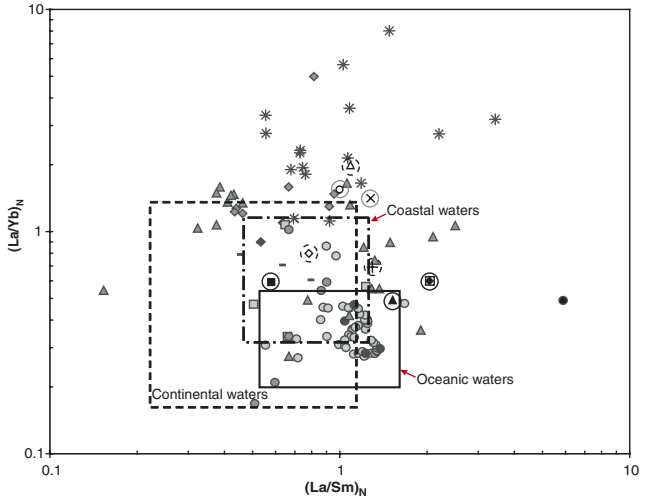

Fig. 7. Compilation of observed $(La/Yb)_N$ vs. $(La/Sm)_N$ in biogenic apatites of various ages and types, and fresh and oceanic waters (based on Reynard et al., 1999). *Jurassic fish and reptile teeth (Picard et al., 2002); ▲, Tertiary and Mesozoic fish teeth (Grandjean et al., 1988; Grandjean and Albaréde, 1989); ◆ Cretaceous reptile and dinosaur bones (Samoilov and Benjamini, 1996) and Jurassic coprolites (Kemp and Trueman, 2002); ○, North Atlantic seawater from 0 to 4000 m depth (Elderfield and Greaves, 1982), Southern Ocean from 0 to 4000 m depth (German and Elderfield, 1990) and North Pacific surface and deepwater (Piepgrass and Jacobsen, 1992); ●, bottom waters (German et al., 1991); □, coastal waters (Elderfield and Sholkovitz, 1987) and coastal waters (Hoyle et al., 1984); −, Scotland river waters (Hoyle et al., 1984); ◍, anoxic waters (Elderfield and Sholkovitz, 1987); and current research, ▲ and ■, *C. carcharias*, ×, *I. hastalis*, ◇, *C. angustidens*, △, *C. auriculatus*, ○, *C. megalodon*, □ and ♦, *O. obliquus*, and +, *C. mantelli*. Oceanic, Coastal, and Continental boxes are based on values given by Reynard et al. (1999). Black circles indicate samples with seawater-like REE_N patterns, gray circles indicate sample with shale-like REE_N patterns, and dashed circles indicate samples with mixed seawater- and shale-like REE_N patterns.

above marine and continental waters, a $(La/Sm)_N$ ratio within coastal and oceanic waters (Fig. 7), and a small negative $Ce_{anom.}$ (less than −0.3). The *C. auriculatus* centrum was deposited in the Brussels Sand in a shelf/nearshore environment (Hooyberghs, 1990; Herman et al., 2000). The REE_N pattern is flattened relative to modern seawater and has a minimum in HREE, which indicates the presences of a diagenetic signature resulting from terrestrial influence of the fluids that have undergone diffusion from the sediments into the water column. As such, this centrum preserves a mixture of the seawater and diagenetic signal at time of deposition. *C. angustidens* (group 2), *C. mantelli* (group 2), and *C. auriculatus* (group 3) centra can be used for paleoceanographic and paleoenvironmental reconstructions, but with caution, because they do have a combination of seawater and diagenetic signals.

The fourth group (Fig. 6D), which consists of *C. megalodon* and *I. hastalis*, shows a minimum at Yb, either flat REE_N pattern or a maximum in the heavy MREE (Gd), and high $(La/Yb)_N$ ratios (Fig. 7). The *C. megalodon* centrum was deposited in sandy siltstone near the current day Kanto Mountains in Japan (Hayashi et al., 2003). The REE_N pattern of this *C. megalodon* is almost completely flat, indicating an extensive diagenetic signature influenced from terrestrial sediment. The *I. hastalis* centrum was deposited in a shallow bay sandstone and has a flat REE_N pattern (strong detrital signature), indicating that the major REE source during early diagenesis was continental/river water. This is supported by fresh-water diatoms in the sediments of the Pisco Formation (Brand et al., 2004). The high $(La/Yb)_N$ ratios in *C. megalodon* and *I. hastalis* (Fig. 7) can likewise be explained by the extensive terrigenous influence (Grandjean et al., 1987). *C. megalodon* and *I. hastalis* do not show any indications of fractionation of REE ("bell-shaped" REE_N pattern). These two centra indicate the quantitative intake of REE during early diagenesis with a strong influence of terrestrial sediments in a near-shore environment. They are not useful in global paleoceanographic reconstruction, although they nevertheless record the diagenetic signature of the local sedimentary environment and confirm marginal marine conditions.

5. Conclusions

While certain variables independently provide information about diagenesis, the simultaneous use of crystalinity index, carbonate content, and elemental concentrations has the potential to more fully elucidate depositional environment and diagenesis. Diagenesis resulted in these seven fossil shark centra the incorporation of a combination of seawater signal, diagenetic signal (diagenetic fluids expelled from sediments), and detrital signal (river water) at the sediment/seawater interface. These seven fossil specimens do not have MREE enrichment, which occurs due to fractionation with seawater during recrystallization of the apatite (Reynard et al., 1999). Instead, the REE seawater signature was incorporated into the biogenic apatite via a transfer (without fractionation) from a short-lived phase made of oxyhydroxides and organic detritus. The diagenetic signature is caused by the development of porewater concentration gradients, which allow fluxes of REE from sediments to seawater (Grandjean et al., 1987). The amount of terrigenous input and therefore the resulting diagenetic signature controls whether the REE_N patterns and $Ce_{anom.}$ reflect the original seawater signal at time of deposition for these fossil shark centra. This is clearly seen for *I. hastalis*, and *C. megalodon*, with centra that have a strong continental diagenetic signature that disrupts the seawater signal and $Ce_{anom.}$. In contrast, the two *O. obliquus* centra preserve the original REE seawater signal at the time of deposition and have no indication of diagenetic signature influenced by terrigneous sediments. The remaining three centra (*C. angustidens*, *C. megalodon*, and *C. auriculatus*) have diagenetic signatures with some influence from terrestrial sediments evidenced by the slightly flattened REE_N patterns. These latter kinds of samples require caution when interpreting $Ce_{anom.}$ because it is difficult to determine how much these anomalies have been overprinted by diagenetic signal. Hence, the lack of a negative $Ce_{anom.}$ does not

necessarily indicate an anoxic environment but may represent a strong continental influence in the depositional environment. In summary, geochemical data from biogenic apatite of fossil marine vertebrates, such as lamnoid sharks, have the potential to be used to understand diagenesis, depositional environments (local controls), and/or paleoceanography (global controls).

Acknowledgments

We thank M. Gottfried, G. Hubbell, C. Jeremiah, S. Witner, D. Nolf, and O. Sakamoto for allowing us to borrow and sample the shark centra. We thank G. Kamenov, A. Heatherington, C. Bohn, and A. Shriller for assistance in the laboratory. C. Lécuyer, T. Lyons, and the other two reviewers provided helpful comments that improved this manuscript. This research was supported by NSF Grant EAR 0418042. This is University of Florida Contribution to Paleobiology 569.

Associate editor: Timothy W. Lyons

References

Ayress, M.A., 1993. Ostracod biostratigraphy and palaeoecology of the Kokoamu Greensand and Otekaike Limestone (late Oligocene to early Miocene), North Otago and South Canterbury, New Zealand. *Int. Symp. Ostracoda* **11**, 676–677.

Barrick, R.E., Showers, W.J., 1994. Thermophysiology of *Tyrannosaurus rex*: evidence from oxygen isotopes. *Science* **265**, 222–224.

Bernat, R.T., 1975. Les isotopes de l'uranium et du thorium et les terres rares dans l'environnement marin. *Cah. ORSTORM Ser. Geol.* **7**, 68–83.

Bonel, G., 1972. Contribution á l' etude de la carbonatation des apatites. II. Synthése et etude des propriétés physico-chimiques des apatites carbonatées du type B. III. Synthése et etude des propriétés physico-chimiques des apatites carbonates dans deux types de sites. Evolution des specters infraouge en function de la composition de apatites. *Ann. Chim.* **7**, 127–144.

Brand, L.R., Esperante, R., Chadwick, A.V., Poma Porras, O., Alomía, M., 2004. Fossil whale preservation implies high diatom accumulation rate in the Miocene-Pliocene Pisco Formation of Peru. *Geology* **32**, 165–168.

Branstetter, S., Musick, J.A., Colvocoresses, J.A., 1987. A comparison of the age and growth of the Tiger Shark, *Galeocerdo cuveri*, from off Virginia and from the northwestern Gulf of Mexico. *Fish. Bull.* **85**, 269–279.

Cappetta, H., 1987. *Handbook of Paleoichthyology, Chondrichthyes II*. Gustav Fisher Verlag, Stuttgart.

Cappetta, H., 1981. Additional à la faune des Sélaciens fossils du Maroc: sur la presence des genres *Heptranchias*, *Alopias* et *Odontorhytis* dans l'Yprésien des Ouled Abdoun. *Géobios* **14**, 53–575.

Carlson, S., 1990. Vertebrate dental structures. In: Carter, J.S. (Ed.), *Skeletal Biomineralization: Patterns, Processes and Evolutionary Trends*, vol. 1. Van Nostrand Reinhold, New York, pp. 531–556.

Dahm, S., Risnes, S., 1999. A comparative infrared spectroscopic study of hydroxide and carbonate absorption bands in spectra of shark enameloid, dentine, and geological apatite. *Calcif. Tissue Int.* **65**, 459–465.

deBaar, H.J.W., Bacon, M.P., Brewer, P.G., Bruland, K.W., 1985. Rare earth elements in the Pacific and Atlantic Oceans. *Geochim. Cosmochim. Acta* **49**, 1943–1959.

Denys, C., Williams, C.T., Dauphin, Y., Andrews, P., Fernandez-Jalvo, T., 1996. Diagenetical changes in Pleistocene small mammal bones from Olduvai Bed 1. *Palaeogeo. Palaeoclim. Palaeoecol.* **126**, 121–134.

Elderfield, H., Upstill-Goddard, R., Sholkovitz, E.R., 1990. The rare earth elements in rivers, estuaries, and coastal seas and their significance to the composition of ocean waters. *Geochim. Cosmochim. Acta* **54**, 971–991.

Elderfield, H., Sholkovitz, E.R., 1987. Rare earth elements in the pore waters of reducing near shore sediments. *Earth Planet. Sci. Lett.* **82**, 280–288.

Elderfield, H., Pagett, R., 1986. Rare earth elements in ichthyoliths: variations with redox conditions and depositional environment. Sci.. *Total Environ.* **49**, 175–197.

Elderfield, H., Greaves, M.J., 1982. The rare earth elements in seawater. *Nature* **296**, 214–219.

Featherstone, J.D., Pearson, B.S., LeGeros, R.Z., 1984. An infrared method for quantification of carbonate in carbonate apatites. *Caries Res.* **18**, 63–66.

Fleet, A.J., 1984. Aqueous and sedimentary geochemistry of the rare earth elements. In: Henderson, P. (Ed.), *Rare Earth Element Geochemistry*. Elsevier, Amsterdam, pp. 343–373.

German, C.R., Elderfield, H., 1990. Application of the $Ce_{anom.}$ as a paleoredox indicator: the ground rules. *Paleoceanography* **5**, 823–833.

German, C.R., Holliday, B.P., Elderfield, H., 1991. Redox cycling of rare earth elements in suboxic zone of the Black Sea. *Geochim. Cosmochim. Acta* **53**, 3179–3183.

Grandjean-Lécuyer, P., Feist, R., Albaréde, 1993. Rare earth elements in old biogenic apatite. *Geochim. Cosmochim. Acta* **57**, 2507–2514.

Grandjean, P., Albaréde, F., 1989. Ion probe measurement of rare earth elements in biogenic phosphates. *Geochim. Cosmochim. Acta* **53**, 3179–3183.

Grandjean, P.H., Capetta, H., Albarede, F., 1988. REE and Nd of 40–70 Ma old fish debris from the West-African platform. *Geophys. Res. Lett.* **15**, 389–394.

Grandjean, P., Cappetta, H., Michard, A., Albaréde, F., 1987. The assessment of REE patterns and $^{143}Nd/^{144}Nd$ ratios in fish remains. *Earth Planet. Sci. Lett.* **84**, 181–196.

Grant, J.A., 1982. The isocon diagram—a simple solution to Gresen's equation for metasomatic alteration. *Econ. Geol.* **81**, 1976–1982.

Greene, E.F., Tauch, S., Webb, E., Amarasiriwardena, D., 2004. Application of diffuse reflectance infrared Fourier transform spectroscopy (DRIFT) for the identification of potential diagenesis and crystallinity changes in teeth. *Microchem. J.* **76**, 141–149.

Hattin, D., 1981. Petrology of Smoky Hill Member, Niobrara Chalk (Upper Cretaceous), in type area, Western Kansas. *AAPG Bull.* **65**, 831–849.

Hayashi, H., Kurihara, Y., Horiuchi, S., Iwashita, T., Yanagisawa, Y., 2003. Planktonic foraminferal biostratigraphy of the Miocene sequence in the Iwadono Hills, Central Japan: an integrated approach. *Palaios* **18**, 176–191.

Henderson, P., Marlow, C.A., Molleson, T.I., Williams, C.T., 1983. Patterns of chemical change during bone fossilization. *Nature* **306**, 358–360.

Herman, J., Steurbaut, E., Vandenberghe, N., 2000. The boundary between the middle Eocene Brussel Sand and the Lede Sand formations in the Zaventem–Nederokkerzeel area (Northeast of Brussels, Belgium). *Geol. Belg.* **3**, 231–255.

Holcomb, D.W., Younf, R.A., 1980. Thermal decomposition of tooth enamel. *Calcif. Tissue Int.* **31**, 189–201.

Hooyberghs, H.J.F., 1990. New palaeoecological studies in benthic foraminifera from the Brussels Sands Formation (Lutetian, Middle Eocene) in Belgium. *Bull. De la Société belge de Geol.* **3**, 337–354.

Hoyle, J., Elderfield, H., Gledhill, A., Greaves, M., 1984. The behavior of the rare earth elements during mixing of river and seawaters. *Geochim. Cosmochim. Acta* **48**, 143–149.

Hubert, J.F., Panish, P.T., Chure, D.J., Prostak, K.S., 1996. Chemistry, microstructure, petrology, and diagenetic model of Jurassic dinosaur bones, Dinosaur National Monument, Utah. *J. Sed. Res.* **66**, 531–547.

Kemp, R.A., Trueman, C.N., 2002. Rare earth elements in Solnhofen biogenic apatite: Geochemical clues to the palaeoenvirnment. *Sed. Geol.* **155**, 109–127.

Koch, P.L., Halliday, A.N., Walter, L.M., Stearley, R.F., Huston, T.J., Smith, G.R., 1992. Sr isotopic composition of hydroxyapatite from recent and fossil salmon: the record of lifetime migration and diagenesis. *Earth Planet. Sci. Lett.* **108**, 277–287.

Koeppenkastrop, D., De Carlo, E.H., 1992. Sorption of rare earth elements from seawater onto synthetic mineral particles: an experimental approach. *Chem. Geol.* **95**, 251–263.

Kolodny, Y., Luz, B., Sander, M., Clemens, W.A., 1996. Dinosaur bones: fossils or pseudomorphs? The pitfalls of physiology reconstruction from apatitic fossils. *Palaeogeog. Palaeoclimat. Palaeoecol.* **126**, 151–160.

Kolodny, Y., Luz, B., 1991. Oxygen isotopes in phosphates of fossil fish- Devonian to Recent. In: Taylor, H.P., Jr.Jr., O'Neil, J.R., Kaplan, I.R. (Eds.), *Stable Isotope Geochemistry: A Tribute to Samuel Epstein*, 3. The Geochemical Society, Special Publication, London, pp. 105–119.

Kolodny, Y., Luz, B., Navon, O., 1983. Oxygen isotope variation in phosphate of biogenic apatites, I. Fish bone apatite-rechecking the rules of the game. *Earth Planet. Sci. Lett.* **64**, 398–404.

Laenen, B., Hertogen, J., Vandenberghe, N., 1997. The variation of the trace-element content of fossil biogenic apatite through eustatic sea-level cycles. *Palaeogeog. Palaeoclimat. Palaeoecol.* **132**, 325–342.

Lancelot, Y., Seibold, E., 1978. The evolution of the Central Northeastern Atlantic: summary of results of DSDP Leg 41. *Initial Report DSDP* **41**, 1215–1245.

Lécuyer, C., Reynard, B., Grandjean, P., 2004. Rare earth element evolution of Phanerozoic seawater recorded in biogenic apatites. *Chem. Geol.* **204**, 63–102.

Lécuyer, C., Grandjean, P., O'Neil, J.R., Cappetta, H., Martineau, F., 1993. Thermal oceanic excursions at the Cretaceous–Tertiary boundary: the $\delta^{18}O$ record of phosphatic fish debris (northern Morocco). *Palaeogeog. Palaeoclimat. Palaeoecol.* **150**, 235–243.

Lee-Thorp, J.A., van der Merwe, N.J., 1991. Aspects of the chemistry of modern and fossil biological apatites. *J. Archaeol. Sci.* **18**, 343–354.

MacFadden, B.J., Labs-Hochstein, J., Quitmyer, I., Jones, D.S., 2004. Incremental growth and diagenesis of skeletal parts of the lamnoid shark *Otodus obliquus* from the early Eocene (Ypresian) of Morocco. *Palaeogeog., Palaeoclimat., Palaeoecol.* **206**, 179–192.

Michel, V., Ildefonse, P., Morin, G., 1995. Chemical and structural changes in *Cervus elaphus* tooth enamels during fossilization (Lazaret cave): a combined IR and XRD Rietveld analysis. *Appl. Geochem.* **10**, 145–159.

Montaser, A. (Ed.), 1998. *Inductively coupled plasma mass spectrometry*. Wiley, New York.

Murphy, K., Dymond, J., 1984. Rare earth element fluxes and geochemical budget in the eastern equatorial Pacific. *Nature* **307**, 444–447.

Nathan, Y., 1981. Structural position of trace elements in apatites: Implications for their recovery. *Isreal J. Earth Sci.* **30**, 31–34.

Nathan, Y., Sass, E., 1983. Stability relations of apatites and calcium carbonates. *Chem. Geol.* **34**, 103–111.

Nelson, D.G.A., 1981. The influence of carbonate on the atomic structure and reactivity of hydroxyapatite. *J. Dental Res.* **60**, 1621–1629.

Nelson, D.G.A., Featherstone, J.D.B., Ducan, J.F., Cutress, T.W., 1983. Effect of carbonate and fluoride on the dissolution behavior of synthetic apatites. *Caries Res.* **17**, 200–211.

Newsley, H., 1989. Fossil bone apatite. *Applied Geochem.* **4**, 233–245.

Picard, S., Lécuyer, C., Barrat, J., Garcia, J., Cromart, G., Sheppard, S.M., 2002. Rare earth element content of Jurassic fish and reptile teeth and their potential relation to seawater composition (Anglo-Paris Basin, France and England). *Chem. Geol.* **186**, 1–16.

Picard, S., Garcia, J.P., Lécyuer, Sheppard, S.M.F., Cappetta, H., Emig, C.C., 1998. $\delta^{18}O$ values of coexisting brachiopods and fish: temperature differences and estimates of paleo-water depths. *Geology* **26**, 975–978.

Piepgrass, D.J., Jacobsen, S.B., 1992. The behavior of rare earth elements in seawater: precise determination of variations in the North Pacific water column. *Geochim. Cosmochim. Acta* **56**, 1851–1862.

Piper, D.Z., 1974. Rare earth elements in the sedimentary cycle: a summary. *Chem. Geol.* **14**, 896–901.

Pucéat, E., Reynard, B., Lécuyer, C., 2004. Can crystallinity be used to determine the degree of chemical alteration of biogenic apatites? *Chem. Geol.* **205**, 83–97.

Reiche, I., Favre-Quattropani, L., Vignaud, C., Bocherens, H., Charlet, L., Menu, M., 2003. A multi-analytical study of bone diagenesis: the Neolithic site of bercy (Paris, France). *Meas. Sci. Technol.* **14**, 1608–1619.

Reynard, B., Lécuyer, C., Grandjean, P., 1999. Crystal-chemical controls on rare-earth element concentrations in fossil biogenic apatites and implications for paleoenvironmental reconstructions. *Chem. Geol.* **155**, 233–241.

Rink, W.J., Schwarcz, H.P., 1995. Tests for diagenesis in tooth enamel: ESR dating signals and carbonate contents. *J. Archaeol. Sci.* **22**, 251–255.

Samoilov, V.S., Benjamini, C., 1996. Geochemical features of dinosaur remains from the Gobi Desert, South Mongolia. *Palaios* **11**, 519–531.

Shemesh, A., 1990. Crystallinity and diagenesis of sedimentary apatites. *Geochim. Cosmochim. Acta* **54**, 2433–2438.

Shields, G., Stille, P., 2001. Diagenetic constraints on the use of cerium anomalies as palaeoseawater redox proxies: an isotopic and REE study of Cambrian phosphorites. *Chem. Geol.* **175**, 29–48.

Sholkovitz, E.R., Landing, W.M., Lewis, B.L., 1994. Ocean particle chemistry: the fractionation of rare earth elemnts between suspended particles and seawater. *Geochim. Cosmochim. Acta* **58**, 1567–1580.

Starton, R.M., Grandstaff, B., Gallagher, W.B., Grandstaff, D.E., 2001. REE signatures in vertebrate fossils from Sewell, NJ: implications for location of the *K–T* boundary. *Palaios* **16**, 255–265.

Stuart-Williams, H.Q., Schwarcz, H.P., White, C.D., Spence, M.W., 1996. The isotopic composition and diagenesis of human bone from Teotiuacan and Oaxaca, Mexico. *Palaeogeog. Palaeoclimat. Palaeoecol.* **126**, 1–14.

Trueman, C.N., 1999. Rare earth element geochemistry and taphonomy of terrestrial vertebrate assemblages. *Palaios* **14**, 555–568.

Trueman, C.N., 1996. Variation of REE patterns in dinosaur bones from North West Montana: implications for taphonomy and preservation. *Geoscientist* **6**, 27–30.

Trueman, C.N., Tuross, N. 2001. Trace elements in recent and fossil bone apatite. In: Kohn, M.L., Rakovan. J., Hughes. J.M. (Eds.). *Phosphates-Geochemical, geobiological, and materials importance* Reviews in Mineralogy and Geochemistry, pp. 489–515.

Trueman, C.N., Benton, M.J., 1997. A geochemical method to trace the taphonomic history of reworked bones in sedimentary settings. *Geology* **25**, 263–266.

Wang, Y., Cerling, T.E., 1994. A model of fossil tooth and bone diagenesis: Implications for paleodiet reconstruction from stable isotopes. *Palaeogeog., Palaeoclimat., Palaeoecol.* **107**, 281–289.

Weiner, S., Price, P.A., 1986. Disaggregation of bone into crystals. *Calcif. Tissue Intern.* **39**, 365–375.

Whittacker, E.J.W., Muntus, R., 1970. Ionic radii for use in geochemistry. *Geochim. Cosmochim. Acta* **34**, 945–956.

Williams, C.T., 1989. Trace elements in fossil bone. *Appl. Geochem.* **4**, 247–248.

Williams, C.T., 1988. Alteration of chemical composition of fossil bones by soil processes and groundwater. In: Grupe, G., Herrmann, B. (Eds.), *Trace Elements in Environmental History*. Springer-Verlag, Berlin, pp. 27–40.

Wright, L.E., Schwarcz, H.P., 1996. Infrared and isotopic evidence for diagenesis of bone apatite at Dos Pilas, Guatemala: Palaeodietary implications. *J. Archaeol. Sci.* **23**, 933–944.

Wright, J., Schrader, H.M., Holser, W.T., 1987. Paleoredox variations in ancient oceans recorded by rare earth elements in fossil apatite. *Geochim. Cosmochim. Acta* **51**, 631–644.